Asymmetric Temporal Properties in the Receptive Field of Retinal Transient Amacrine Cells

Kaj Djupsund,[1,2] Tetsuo Furukawa,[3] Syozo Yasui,[4] and Masahiro Yamada[1]

[1]Department of Production, Information and Systems Engineering, Tokyo Metropolitan Institute of Technology, Hino, Tokyo 191-0065, Japan

[2]University of Kuopio, Department of Neuroscience and Neurology, FIN-70211 Kuopio, Finland

[3]Kyushu Institute of Technology, Iizuka, Fukuoka 820, Japan

[4]Graduate School of Life Science and Systems Engineering, Kyushu Institute of Technology, Kitakyusha 808-0916, Japan

ABSTRACT The speed of signal conduction is a factor determining the temporal properties of individual neurons and neuronal networks. We observed very different conduction velocities within the receptive field of fast-type On-Off transient amacrine cells in carp retina cells, which are tightly coupled to each other via gap junctions. The fastest speeds were found in the dorsal area of the receptive fields, on average five times faster than those detected within the ventral area. The asymmetry was similar in the On- and Off-part of the responses, thus being independent of the pathway, pointing to the existence of a functional mechanism within the recorded cells themselves. Nonetheless, the spatial decay of the graded-voltage photoresponse within the receptive field was found to be symmetrical, with the amplitude center of the receptive field being displaced to the faster side from the minimum-latency location. A sample of the orientation of varicosity-laden polyaxons in neurobiotin-injected cells supported the model, revealing that ~75% of these processes were directed dorsally from the origin cells. Based on these results, we modeled the velocity asymmetry and the displacement of amplitude center by adding a contribution of an asymmetric polyaxonal inhibition to the network. Due to the asymmetry in the conduction velocity, the time delay of a light response is proposed to depend on the origin of the photostimulus movement, a potentially important mechanism underlying direction selectivity within the inner retina.

KEY WORDS: carp • latency • conduction velocity • direction selectivity

INTRODUCTION

Previous studies have indicated that the mechanisms underlying direction selectivity in the inner retina are attributable to an interaction between asymmetric inhibitory and excitatory processes and are initiated by the motion of an object in the visual field (e.g., Barlow and Levick, 1965; Taylor et al., 2000; Borg-Graham, 2001; Euler et al., 2002; Fried et al., 2002). Thus, an observed spatial asymmetry in ganglion cells could be the result of a presumed earlier underlying temporal asymmetry, namely the timed or coincident arrival of signals from several sources onto the ganglion cell dendrites. Since this implied that a mechanism for temporal signal control could reside at or before the level of ganglion cell processing, we studied the presynaptic cell layer, the network of electrically coupled fast On-Off type transient amacrine cells (TACs).

In carp, the majority of TACs have a relatively small bushy primary dendritic field with a sparse polyaxonal network extending further out, whereas a few cells have only large primary dendritic fields (Teranishi et al., 1987; Djamgoz et al., 1990; Völgyi et al., 2001). Functionally, these TAC groups can be recognized according to the rise and decay time of their transient depolarizations, without predominant DC components, to steps of light, which divides the cells into two classes, fast and slow TACs (Teranishi et al., 1987). The depolarizing response is a form of EPSP, mainly due to calcium currents with the involvement of secondary sodium currents (Watanabe and Murakami, 1985; Koizumi et al., 2001). Direct two-electrode measurements show that inputs feeding On- and Off-responses come from different pathways, from On- and Off-bipolar cells, respectively (Kujiraoka et al., 1988).

The fast-type TACs (hereafter "TAC" for simplicity) are tightly coupled to each other via strong tip-to-tip or tip-to-side gap junctional contacts, which have been demonstrated with both dye and tracer coupling (Teranishi et al., 1987; Negishi et al., 1991). These observations match the wide receptive field, which exceeds the dendritic field of these cells (Kaneko, 1973; Teranishi et al., 1987; Negishi et al., 1991). In addition, TAC cou-

Address correspondence to Masahiro Yamada, Department of Production, Information, and Systems Engineering, Tokyo Metropolitan Institute of Technology, 6-6, Asahigaoka, Hino, Tokyo 191-0065, Japan. Fax: (81) 42-583-5119; email: myamada@cc.tmit.ac.jp

Abbreviations used in this paper: GABA, γ-aminobutyric acid; TAC, transient amacrine cell.

J. Gen. Physiol. © The Rockefeller University Press • 0022-1295/2003/10/445/14 $8.00
Volume 122 October 2003 445–458
http://www.jgp.org/cgi/doi/10.1085/jgp.200308828

pling has been reported to be restricted to cells of the same subtype (Negishi et al., 1991; Hidaka et al., 1993). Thus, they form diffuse lateral networks (Naka and Christensen, 1981; Marc et al., 1988; Negishi et al., 1991). Also, because of the strong electrical coupling within the bushy dendritic network of these cells, synaptic current flow will not be restricted within only a few narrow dendrites, a necessary condition for electrically autonomous subunits (Goldstein and Rall, 1974; Ellias and Stevens, 1980; Miller and Bloomfield, 1983; Bloomfield, 1992, 1996).

These TACs constitute a well-known group of cyprinid amacrine cells. They provided an excellent system for studying lateral spread of signals in the receptive field of a large cellular network. This signal spread was measured in the form of latency and amplitude profiles. The latency profiles provided the measure for conduction velocity, which was found to be highly asymmetrical and the asymmetry appeared to be located within the TAC network itself. A corresponding directional asymmetry was found in the anatomy of the polyaxonal network of these cells and a model, based on an asymmetric polyaxonal inhibition, was constructed to explain the results. A part of this paper has previously been published in abstract form (Djupsund and Yamada, 1997).

MATERIALS AND METHODS

Recordings

Intracellular recordings were obtained from flat-mount retina of light-adapted, 20–25-cm carp (*Cyprinus carpio*), which were dark-adapted for 5–10 min and pithed. After removal and hemisection of the 12–14 mm eyeball under dim red light, the retina was attached to a black filter paper (No. 131B; Toyo Roshi) with the photoreceptor-side up and superfused with physiological Ringer solution (e.g., Yamada and Saito, 1997), saturated by 95% O_2–5% CO_2 gas mixture. All procedures were made at room temperature, 20–22°C. Most of the microelectrodes were filled with 3 M potassium chloride, their resistances being 200–500 MΩ, and the penetrations were made avoiding the peripheral edges of the retina, at least 2 mm from the edge. The penetrations started >20 min after preparation, allowing the retina to stabilize and adapt to steady-state. The TACs were consistently found at a recording depth of 150–200 μm and the subtypes were determined by temporal response characteristics to flash stimuli. The response waveform of fast-type TACs (Fig. 1 B) is unique, with depolarizing responses to on- and off-set of photostimuli. Thus, all analyses in this work are based on the transient depolarizations. The recorded data were stored on a digital audio tape and, thereafter, digitized and saved on a hard disk in a personal computer.

Intracellular Labeling

A number of cells were intracellularly stained with Lucifer yellow (n = 12, 3% in 1 or 0.1 M LiCl) for anatomical identification, or by an iontophoretical injection of neurobiotin (n = 6, yielding ~140 cells with apparently completely stained primary dendrites; Vector), in order to verify both gap junctional coupling within the network (Hidaka et al., 1993) and the direction of the axons. The electrodes used for staining were thicker than those for the ordinary recordings, had resistances of 80–300 MΩ and contained either 3–5% neurobiotin in 1 M KCl or a mixture of neurobiotin and Lucifer yellow in 1 or 0.1 M LiCl. The outermost tip was filled with the aid of a micro-capillary reaction. The proximal part of the capillary was back-filled with the medium solution. During the experiment, the retina was kept in darkness for 40 min to allow diffusion of the tracer, after a 1-min injection of +2 nA pulsed current. The neurobiotin-injected retinae were immunohistochemically treated with a Vectorstain ABC solution (PK-4000; Vector) in the presence of 1% Triton X-100. 0.05% diaminobenzidine (DAB), 0.025% nickel ammonium sulfate, and a few drops of 0.3% H_2O_2 were subsequently used to finish the staining process. All procedures were performed in 0.1 M phosphate buffer (pH 7.4). A Nikon OptiPhoto2 and Olympus BX51WI microscope both with PlanApo series objective lenses were used for the counting of the axons and to determine their direction in the retina.

Light Stimulation

The light stimuli were either white slits (110 or 220 μm wide, 7 mm long) or spots and annuli. For the annuli, the illuminated area covered the whole retina except for the central hole. All stimuli were produced and their dimensions determined by a computer-controlled projector system, rearranged from a liquid crystal display projector (Epson, ELP-3300) using a 150-W metal halide lamp. All stimuli were presented in flashes of 700-ms duration at 4.5-s intervals. The use of a slit allows one to simplify the analysis of the TAC network response into a one-dimensional situation, as has been demonstrated previously both theoretically and experimentally (Lamb and Simon, 1976; Yamada and Saito, 1997). The consecutive positions of the center of slits were 90–150 μm apart on the retina, along one or several axes in the receptive field. All stimuli were imposed on a diffuse white background light (intensity 3×10^{-7} W/cm^2 at 513 nm, measured by a PIN-diode, type 1227, Hamamatsu Photonics) illuminating the whole retina. The intensity of all stimuli was 2.4 log-units above the background; no other stimuli were used before or between the scanning procedures. The total intensity was adjusted to produce nonsaturating responses, when the slit stimuli were applied. Before the recording session, one test electrode was aligned to the center of the spot/annulus under the microscope (Nikon TMD).

Analysis of Data

The latency and amplitude data of responses were collected off-line. Usually, the recording and analysis contained several sets of data at each stimulus position; the averages of these datasets were used for analysis. The On- or Off-response latency was determined as the time from the stimulus onset or offset of pulsed photostimuli, respectively, to the first response peak. Conduction velocity was measured as a ratio between retinal displacement of stimuli and the latency of responses. In annulus recordings, the retinal displacement of the stimulus was determined by the relative distance of the annulus inner edge. In slit recordings, the conduction velocity was determined by the reciprocal value of the slope of the linear regression line, fitted to the latency data in each side (one-axis scans) or in each sector (multi-axis scans) of the receptive field center. This definition is similar to that used for the conduction velocity of action potentials.

We ruled out the possibility that our results would be affected by any second-order effects of moving stimuli, such as long-term photoreceptor or postphotoreceptor adaptation (Donner et al., 1991; Smirnakis et al., 1997; Shiells and Falk, 2000), by comparing five recordings with consecutive scanning and random scan-

ning, where the slit jumped from one randomly chosen location to another. The obtained latencies and conduction velocities differed by less than ±5% from each other in all cases.

The size of the receptive field was measured as the distance between the two furthermost slits from the recording site eliciting a criterion voltage response (two standard deviations above the noise band in the recording, usually 1–1.5 mV). The amplitude data, when the stimulus was kept at a nonsaturating level, was fitted with an exponential decay function, $V(x) = a \cdot e^{-x/\lambda}$, toward both sides from the receptive field center defined as a location responding with the largest amplitudes. Here $V(x)$ is the response amplitude at distance x on the retina from the receptive field center, a is a fixed constant and λ is the obtained space constant (length constant), which effectively describes the spatial decay toward a receptive field edge. This type of fitting was adopted from previous similar approaches in carp horizontal (Yagi, 1986; Yamada et al., 1992) and bipolar cells (Yamada and Saito, 1997).

The retinal dorsal direction is defined as 0 ± 45 degrees and ventral direction as 180 ± 45 degrees from zenith, all other directions are considered as horizontal. For the counts of polyaxons, only varicosity-laden processes were used.

All results are presented as mean ± SEM, with statistical comparisons by paired or nonpaired Student's t-tests in Origin 4.1 (Origin International, Inc.) or Prism 2 (GraphPad Software, Inc.).

RESULTS

We recorded from 117 TACs of which 89 were classified as fast- and 28 as slow-type TACs (similar to the ratio of fast to slow TACs reported by Teranishi et al. [1987]). In 16 penetrations, TACs were labeled with neurobiotin or Lucifer yellow or both by the injections after recording the photoresponses to slit or diffuse light stimuli for identification. Of the fast-type TACs, 22 yielded long enough recordings for the analysis of conduction velocity through latency profiles using slit stimuli. In

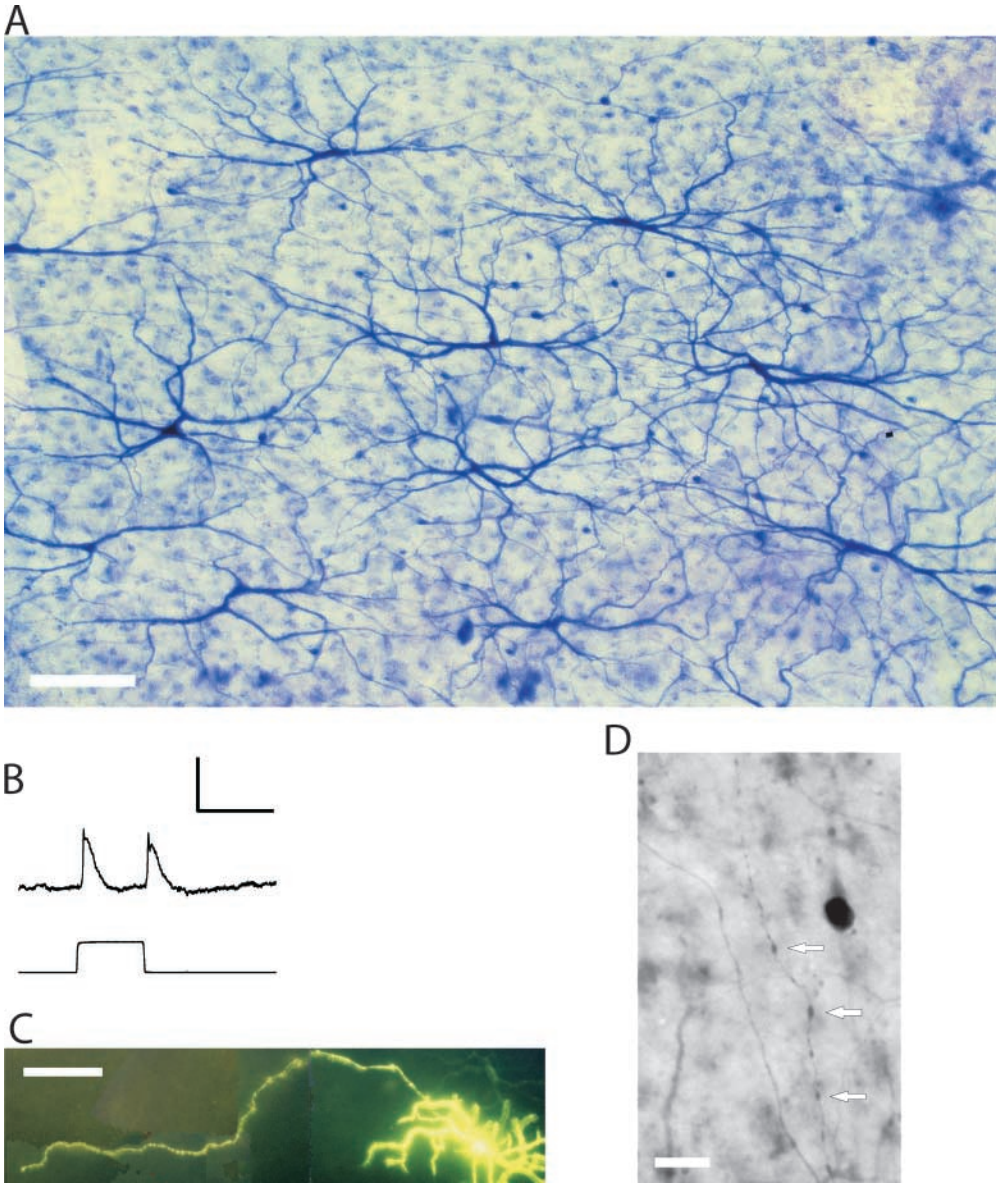

FIGURE 1. Fast-type TACs in an isolated retina of carp. (A) A group of TACs, as stained by an intracellular injection of neurobiotin into a single TAC and the diffusion of the neurobiotin through gap junctions between the cells in the group. Several distinct, but more faintly labeled cell populations can be seen from the center toward the top right. A number of varicosity-laden processes can be seen under higher magnification (D) in this network and directed mainly toward the lower right corner. Scale bar, 100 μm. (B) The photoresponse of the injected cell, as recorded before staining. The cell responded with a depolarization to an On- and Off-set of a diffuse photostimulus. Bars: 10 mV and 700 ms. (C) A single TAC with an extended axonal process, stained with Lucifer yellow. The direction of this process was ~45 degrees from the dorsal toward the rostral. Bar, 100 μm. (D) One varicosity-laden process under higher magnification. Varicosities, white arrows. Note the large difference compared with an adjacent process without varicosities. Bar, 10 μm.

most cases, we initially used the centered spot and annular stimuli to establish a measure of the conduction velocity along the retinal plane. Secondly, we obtained the conduction velocities with slit stimuli applied along one or several axes within the receptive field. Finally, we assessed offline the spatial decline of the response amplitudes and compared how temporal and amplitude properties corresponded to each other.

The Morphology of TAC Networks

An example of a neurobiotin-stained TAC network and its photoresponse is shown in Fig. 1. In this network, most primary processes of TACs can be seen to be elongated along a common axis. The dendritic processes of these cells were bi-stratified (sublaminas *a* and *b*), as has been reported to be the typical morphology of TACs. An example of the response waveform of fast-type TACs can be seen in Fig. 1 B, consisting of depolarizing responses without predominant DC components at the on- and off-set of a photostimulus (this response is from the impaled network in Fig. 1 A). Around the center of the stained area we occasionally observed up to five distinct, but more faintly labeled cell populations, which resided in- and outside the sublaminae occupied by TAC dendrites (Fig. 1 A).

In addition to the main morphology, varicosity-laden axonal processes were counted (Fig. 1, C and D). The average diameter of the primary dendritic field was 240 μm (236 ± 11 μm, $n = 28$), the average length of visible axonal processes was ~700 μm and their average varicosity interval ~20 μm. One end of the process could be seen to arise from a primary dendrite branch, the other end of a process could be seen as a sparse, branching formation ~5 μm in length, extending from the process.

The directionality of varicosity-laden processes was assessed in three TAC networks. The processes were defined on the basis of their diameter (<1 μm), length (average 700 μm) and presence of varicosities. Not all cells in the networks exhibited varicosity-laden processes; in only 28 of our 140 cells were such processes seen. Whether this was due to incomplete staining or a real rarity is unclear. On average in these cells, 1.2 ± 0.2 varicosity-containing axons could be found to extend from the primary dendrites or soma. In total, 33 processes were found, 24 extending toward the dorsal side of the stained cell, 7 toward the ventral side, and 2 were horizontal. Thus, the varicosity-laden processes showed a strong directionality.

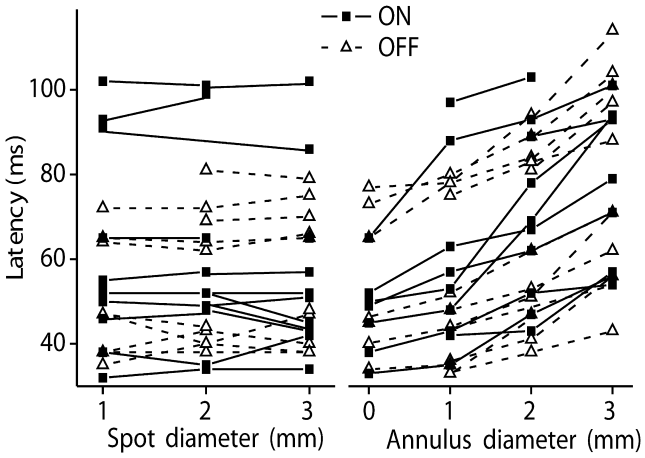

FIGURE 2. Comparison of response latencies of TACs to spot and annulus irradiation, as restricted to responses of similar amplitude (±10% of average in each set). (A) Independence of response latencies of spot size. The latency was determined as the time from the stimulus onset or offset to the first response peak. The response latency was essentially the same for different spot diameters. (B) Dependence on the inner diameter of the annuli, ranging from 0 to 3 mm. The response latency increased with diameter. The data at diameter 0 were those responses to spots from A, fulfilling the amplitude criterion. The outer diameter was 12 mm in all cases.

Spot and Annulus Experiments

Conduction velocities estimated at equal-amplitude responses. The response latency was defined as the time to response peak from stimulus onset or offset. For the measurement of response latencies to annular and spot stimuli, only responses with the same amplitude

TABLE I

The Conduction Velocities of Fast-type TACs, as Determined from Annular and Slit Stimuli

	On- and Off-response conduction velocity (mm/s)	
	On	Off
Annular stimuli	114 ± 23 ($n = 26$)	108 ± 21 ($n = 26$)
Single scan (faster half)	75 ± 17 ($n = 12$)	75 ± 19 ($n = 12$)
Single scan (slower half)	23 ± 3 ($n = 12$)	25 ± 3 ($n = 12$)
Multiple scan (max speeds)	102 ± 34 ($n = 10$)	117 ± 36 ($n = 10$)
Multiple scan (min speeds)	13 ± 3 ($n = 10$)	21 ± 7 ($n = 10$)

The conduction velocity determined from annuli was calculated as the difference of two inner radii of the two annular light stimuli divided by the time difference of the response latencies. In slit recordings, the conduction velocities were calculated from the linear regression line of the response latencies. For single scans, a receptive field half was classified as a faster or a slower half based on the measured conduction velocity. Data are shown as mean ± SEM.

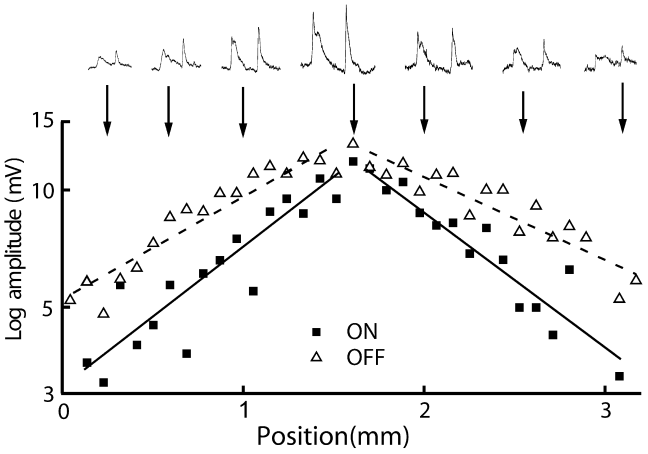

FIGURE 3. Receptive field profile of a TAC, as measured by slit stimuli. (Top) Responses to flashed slit stimuli (700 ms duration and 4.5-s intervals), as located at various distances from the recording electrode. (Bottom) The spatial decay of On- and Off-response amplitudes, as a function of the displacement from the apparent field center. The length constants to the left and right were for On-responses 0.79 and 0.68 mm and those for Off-responses 1.22 and 1.57 mm, respectively.

(±10%) were used in order to exclude combined effects of latency and amplitude.

The latencies to spot stimuli did not change with spot diameter, as shown in Fig. 2 A. The average latency of On-responses was 59 ± 4 ms (n = 31), indistinguishable from the Off-response latencies (53 ± 3 ms, n = 31). The latency of responses to annuli, however, increased with the inner diameter of the annulus (Fig. 2 B). The conduction velocity was determined by the ratio between the difference of inner radii of the two annular light stimuli and the time difference of the response peak latencies. The obtained conduction velocities were 114 ± 23 mm/s for On- and 108 ± 21 mm/s (n = 26) for Off-responses, as shown in Table I.

Slit Experiments

The spatial decay of amplitudes in the receptive field. The photoresponse amplitude declined as a function of the distance of the light slit from the recording electrode, toward the receptive field edges (Fig. 3), similarly as in more distal retinal neurones (Yamada et al., 1992; Yamada and Saito, 1997), when slits with nonsaturating intensities were used. The receptive field size, as defined by the distance between the two furthermost slits eliciting a criterion voltage response (two standard deviations of membrane noise), was 2.4 ± 0.2 and 2.6 ± 0.3 mm in diameter for the On- and Off-responses (n = 12), respectively. This indicated that on average 11 cells were contained within one receptive field, as estimated from the size of their primary dendritic field and assuming a low coverage factor, as in Fig. 1 A.

The amplitude data was fitted with an exponential decay function on each side (two lines for On- and Off-responses in Fig. 3, respectively), when the stimulus was kept at a nonsaturating level. The space constant was obtained from the linear regression line of the decay function. On average, the space constant was 0.72 ± 0.06 mm for On- and 0.94 ± 0.11 mm for Off-responses (n = 24).

Latency Profiles and Conduction Velocities in the Receptive Field—One Axis Scans

First, we recorded photoresponses to a slit scanning along one axis. In these experiments, the retinae had a

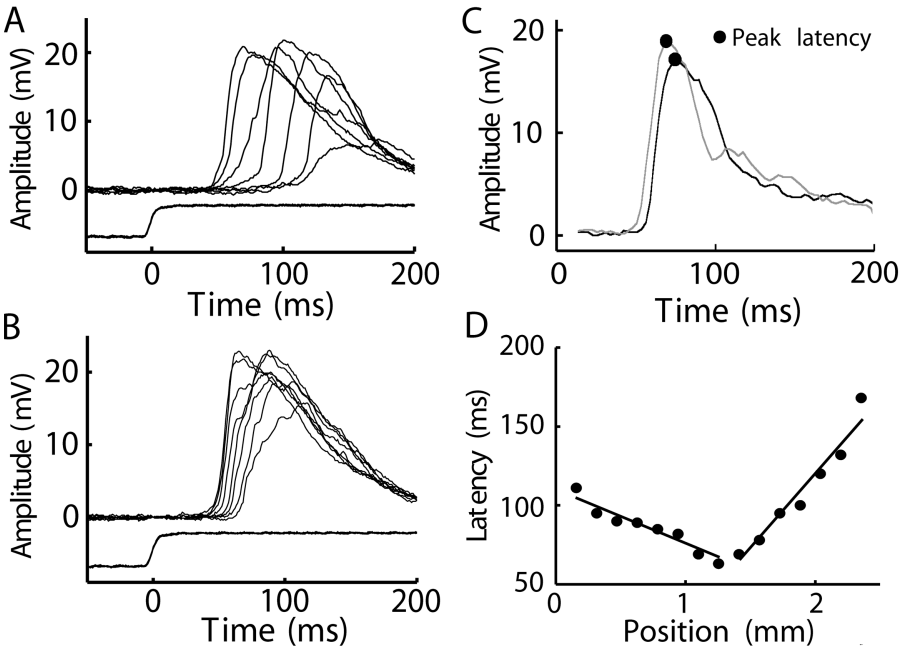

FIGURE 4. Latency and conduction velocity of photoresponses in a TAC measured to slit stimuli as a function of the position on the retina. (A) On-photoresponses at consecutive positions (150-μm steps) in one half of the receptive field, as defined from the apparent amplitude field center. (B) The corresponding responses in the other half. (C) Comparison of a pair of On-photoresponse waveforms at the same distance but in opposite sides. (D) The latencies of the cell in A and B, as defined by the time to the response peak, were plotted against the position of the center of the slit on the retinal surface. Conduction velocities were determined by the reciprocal value of the slope of the linear regression lines (straight lines) along the recorded axes in the receptive field. In this cell, the conduction velocities were 33 and 10 mm/s to the left and to the right, respectively.

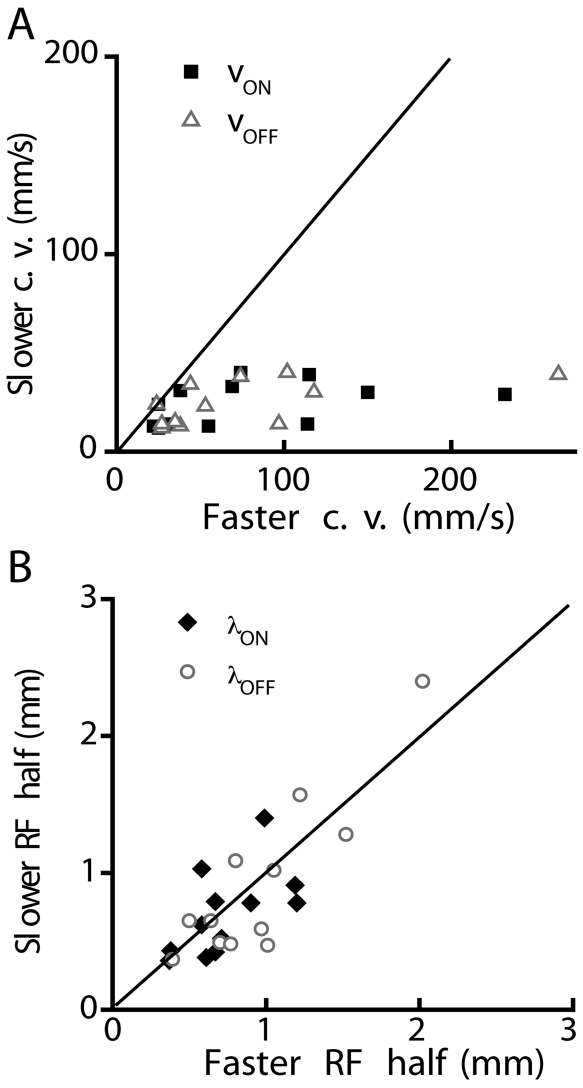

FIGURE 5. Comparison between the conduction velocity asymmetry (A) and the space constant symmetry (B). (A) The degree of asymmetry of conduction velocity between opposite receptive field halves in one-axis scans (n = 12). Each symbol denotes the relation between the faster and slower conduction velocity for On- (filled squares) or Off- (open triangles) responses in each network. The line corresponds to fully symmetric cases, where the conduction velocities of On- or Off-responses on both sides of the recording site were identical. (B) The relation between the length constants λ in opposite receptive field halves of the same cells (black diamonds, On-responses; gray circles, Off-responses), grouped as in A, faster versus slower side. The space constants on both sides of a given receptive field did not significantly differ from each other (paired t test, P = 0.48, n = 24).

random orientation in the setup. The average minimum latencies, the shortest latencies in each recording, were 70 ± 7 and 92 ± 16 ms (n = 12) for the On- and Off-responses, respectively.

We could determine a pair of conduction velocities for On-responses and for Off-responses along each recorded axis of the receptive field. The average of their velocities was 51 ± 8 mm/s (n = 48). In most cells, the pairs of conduction velocities, however, were quite clearly asymmetric on each side of the receptive field. This could be seen when we compared response waveforms and latencies at different locations in opposite sides, but located at equal distances from the receptive field center, as shown in Fig. 4, A and B (On-responses only). Fig. 4 C shows a comparison of a single pair of On-photoresponses at the same distance, but from opposite sides of the field center. When all measured latencies in a recording sequence were plotted out as a profile, a systematic difference was obvious, as shown in Fig. 4 D and Table I. Over all cells, the slower and the faster halves of the receptive field for the On-responses had average speeds of 23 ± 3 and 75 ± 17 mm/s (n = 12), respectively, and those for the Off-responses 25 ± 3 and 75 ± 19 mm/s (n = 12). These differences between the slower versus faster speeds were highly significant (P < 0.002 for On- and P < 0.001 for Off-responses, paired t test).

The asymmetry of the conduction velocities is shown in Fig. 5 A; the 45 degree line corresponds to fully symmetric cases. On average, the conduction velocities showed around a threefold difference, their ratio being 3.5 ± 0.7 for On-responses and 3.3 ± 0.6 (n = 12) for Off-responses. The ratio between Off- to On-conduction velocities in a given receptive field half did not differ significantly from unity (1.04 ± 0.05, n = 24; P = 0.76, paired t test). On the other hand, when the receptive field halves were grouped according to the slower and faster side division in conduction velocity, the space constants were not significantly different from each other (Fig. 5 B, paired t test, P = 0.48, n = 24). This implied that the functional receptive field of these cells was roughly circular-symmetric with respect to its amplitude properties.

Latency Profiles and Conduction Velocities in the Receptive Field—Multiaxis Scans

We analyzed a set of 10 cells using scans along four different axes at 45 degree intervals, with at least two trials for each cell. The precise orientation of the retina was determined in eight cases. The averages of maximum and minimum speeds for the On-responses were 102 ± 34 and 13 ± 3 mm/s, respectively, and those for the Off-responses 117 ± 36 and 21 ± 7 mm/s (n = 10). The asymmetry of conduction velocity was also expressed as the ratio between the velocities along each axis. These multiaxis velocities showed an approximately fivefold difference, the average maximum ratio being 4.9 ± 1.2 for the On-responses and 5.2 ± 0.9 for the Off-responses (n = 10). Fig. 6 A is the normalized conduction velocity ratio along different angles, averaged by adjusting the peak speed of each cell (n = 10) to occur at a position of 45 degrees. The velocity distri-

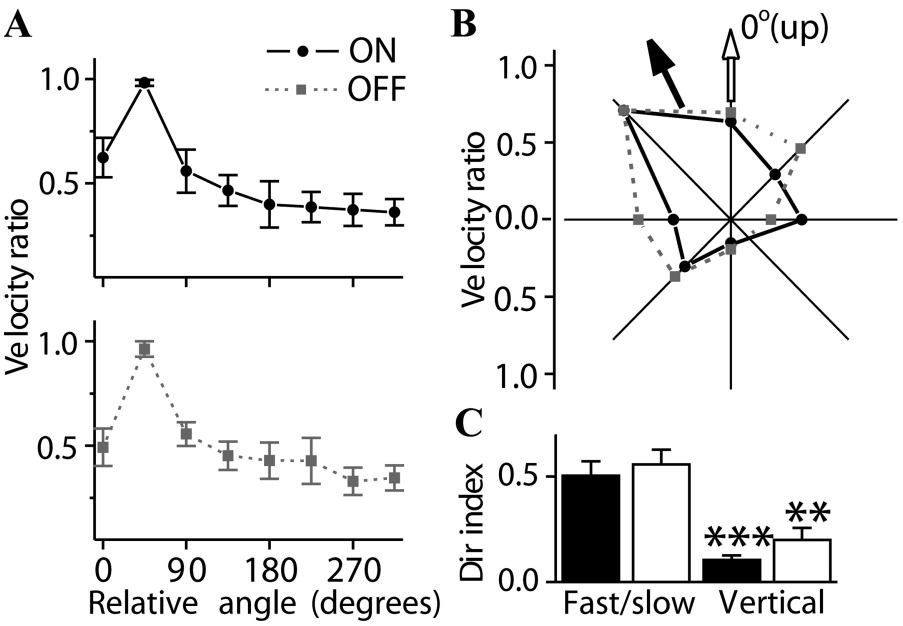

FIGURE 6. Directionality of conduction velocity. The conduction velocity profiles, as obtained from multiple scans along different axes with 45 degree steps. (A) The distribution of On- and Off-velocity, as shown by the normalized ratio to the maximum speed over the different orientations (n = 10). The velocity maxima were adjusted to a relative angle of 45 degrees. (B) Lines: A representative record (solid line: On-velocity, dashed line: Off-velocity) from a TAC with a clear maximum at around 45 degrees. The profiles are normalized to the highest velocity in the record. Arrows: the average velocity maxima for all records (black arrow, On-velocity; white arrow, Off-velocity, n = 8), as in the retinal field. Upward corresponds to the dorsal direction and the angles denotes anti-clockwise rotation to the rostral direction. All velocity maxima were directed upwards from or along the horizontal line from the receptive field centers. No well-defined location was found for velocity minima. (C) The directionality index. The index was calculated as $(x - y)/(x + y)$, where x and y represent the larger and smaller values in a pair of conduction velocities along the four recorded axes. The axis with the largest speed difference was used for the "fast/slow" index and the axis vertical to that as the comparison, i.e., the "perpendicular" axis. Columns and error bars indicate mean ± SEM. The directionality indexes between these two axes were significantly different, for On-velocity (white bar: ***$P < 0.001$, n = 8, paired t test) and Off-velocity (black bar: **$P < 0.005$, n = 8). Thus, On- and Off-indexes in the same groups are indistinguishable.

butions formed a sharp peak against a relatively uniform background, without any clear minimum. The direction of all the velocity maxima was above or on the horizontal midline of the retina (Fig. 6 B). The average direction of the maximum speed was 22.5 degrees and 0 degrees for On- and Off-responses (n = 8), respectively, as counted from the zenith toward the rostral side. To obtain a measure for the degree of velocity profile, we calculated a directionality index, as applied from extracellular ganglion cell recordings (Masland and Ames, 1976; Ariel and Daw, 1982). The index was calculated as $(x - y)/(x + y)$, where x and y represent the larger and smaller value in a pair of conduction velocities along the four recorded axes. The axis with the largest speed difference was used for the "fast/slow" index and the axis vertical to that as the comparison, i.e., the "perpendicular" axis. In themselves and as grouped according to the directionality index, the differences in the velocities within the receptive field were highly significant for On- and Off-responses (levels $P < 0.001$ and $P < 0.005$, respectively, as shown in Fig. 6 C).

The Location of the Receptive Field Center—Amplitude Versus Latency

We could determine the receptive field center for both the latency and amplitude profiles. The faster halves were longer than the slower halves, on average by 370 μm (n = 24), as shown in the example in Fig. 7. When we superimposed the field centers, the location of the latency center was on average displaced 185 μm toward the slower half of the receptive field. The displacement between the location of the amplitude center and the latency center was close to 200 μm, as shown in Table II.

DISCUSSION

Comparison of Conduction Velocity Measurements

The present approach is novel in itself, as most measurements of conduction velocity have been performed on cells or networks with sodium action potentials. In the visual system, these studies have been used for the classification of ganglion cells, both in goldfish On- and Off-cell axons (Northmore and Oh, 1998) and in X, Y, and W cells of cat and monkey retina (Stone and Freeman, 1971; Hsiao et al., 1984; Fukuda et al., 1988). As far as we are aware, the only previously published work not based on action potentials within the visual system is from recordings in turtle photoreceptors (Detwiler et al., 1978). Compared with action potential recordings, the velocities obtained in our study were much lower, being approximately one-tenth to one-hundredth of action potential velocities. Thus, the main speed determinants in TAC-receptive fields are either different or are strongly modified by

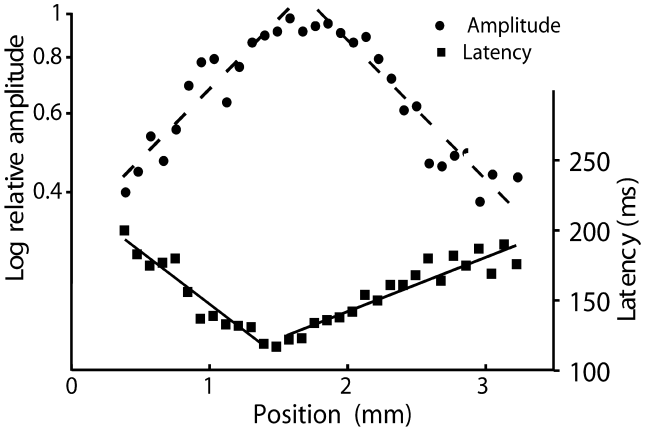

FIGURE 7. A comparison of the locations of the latency center and the amplitude center of a TAC. Squares, response latency; circles, amplitude (On-responses). Left y-axis, amplitude. Right y-axis, latency. Space constants on the left and right side of receptive field were 1.08 and 1.13 mm. Conduction velocities in the left and right side of receptive field were 13 and 28 mm/s, respectively. Before fitting, the amplitudes were averaged with 3- or 5-point adjacent averaging. The location of the latency center was determined by the intersection of the regression lines for the conduction velocity. The center of the amplitude was similarly determined by the intersection of the regression lines for the fit by the exponential decay function. For this cell, a displacement of ~200 μm between these two centers could be seen.

TABLE II

The Receptive Field Size of Each TAC and the Displacement of the Location of the Amplitude Centre in the Receptive Field

Cell #	ON response		OFF response	
	Receptive field size	Displacement	Receptive field size	Displacement
	mm	*mm*	*mm*	*mm*
1	2.0	0.30	2.0	0.30
2	2.4	0.40	2.4	0.25
3	3.1	0.00	3.1	0.10
4	2.5	0.45	2.6	0.30
5	2.6	0.20	2.6	0.15
6	1.8	0.00	1.8	0.15
7	3.9	0.12	5.0	0.05
8	1.8	0.10	2.3	0.00
9	2.3	0.15	3.15	0.15
10	2.0	0.25	2.0	0.20
11	1.5	0.10	1.5	0.05
12	3.0	0.20	3.0	0.20
$n = 12$	2.4 ± 0.2	0.19 ± 0.04	2.6 ± 0.3	0.16 ± 0.03

The receptive field size was measured as the distance of the two furthermost locations of slit eliciting a criterion response voltage. The displacement was the eccentricity of the amplitude centre in relation to the latency centre, both determined by the intersection of regression lines.

one or several factors. The average values for the maximal speeds in one-axis scan slit recordings were lower than those in multiaxis scans, since the scanning axis in the one-axis scan was chosen at random. Thus the average angle between the scanning axis and the axis with a maximum velocity is 45 degrees within these receptive fields. This is close to the geometric relation (i.e., arctan-relation) of the average speed values in one-axis scan compared with our other methods, multiaxis scan recording and annulus experiments.

Directional Asymmetry in Conduction Velocity

We have described the asymmetries on the basis of their latency profiles, absolute velocities, velocity ratios, or a directionality index (Fig. 6 C). The index is adopted from extracellular ganglion cell recordings (Masland and Ames, 1976; Ariel and Daw, 1982) and represents a common tool. Originally the index, however, was a mathematical calculation based on spike rate-coding, reflecting the difference of the arrival of excitatory and inhibitory signals, whereas the conduction velocity was a purely temporal parameter. Also, the responses for directional selective ganglion cells follow a preferred-null pattern (with intermediate-strength responses at stimuli from other directions). This is not necessarily the case here, as can be seen from Fig. 6 A, where the main feature is the single high-velocity peak, which is highlighted against a statistically uniform low-speed background, shown by a broad valley; in analogous terms, a preferred-only or null-only situation. Therefore, the directionality index must be used with caution.

Similarity in Asymmetry of Conduction Velocity in On- and Off-Pathways

As the measured latency reflects the sum of several processes within the distal retina, all these potentially affect the conduction velocities. Furthermore, it has been shown by direct two-electrode measurements that the inputs feeding the On- and Off-responses originate from different pathways, from the On- and Off-bipolar cells, respectively (Kujiraoka et al., 1988). Our findings, however, support the idea that the main factors for the temporal asymmetry reside within the TAC networks themselves, as the latency profiles were similar for the On- and Off-responses in the same area of the receptive field, suggesting that they have a common origin. Therefore, one can assume that the reasons for the asymmetry in the conduction velocity would be located where the visual signal traverses the common part of the On- and Off-pathways, i.e., at the level of the photoreceptors or in TAC themselves. To our current knowledge, however, the photoreceptor layer in carp is homogenous, as reflected in cone density counts and horizontal cell responses, allowing no large variety in the density of the same cone types (Stell and Harosi, 1976; Hack and Peichl, 1999). TAC networks themselves probably contain the major mechanisms accounting for a temporal asymmetry.

The Displacement of Amplitude Center

We detected a distinct difference in the locations between the amplitude and latency centers. One can, however, note that analogous displacements have been found before, e.g., between the receptive and the dendritic field locations in single rabbit ganglion cells (Yang and Masland, 1994). Here, we are dealing with a network and not a single cell. In previous studies, the appearance of individual TACs has been shown to include distinct thick and thin dendritic branches (Teranishi et al., 1987; Djamgoz et al., 1990). Amacrine cells in other fish species do form dendritic fields with a parallel, oriented arrangement of the soma and main dendritic branches (catfish: Naka, 1980; gourami: Sakai et al., 1997). Morphological studies (Teranishi et al., 1987; Hidaka et al., 1993) have revealed that the primary dendritic fields of carp TACs are often, but not always, elongated but symmetric, which agrees with our data of receptive field profiles of the response amplitude. A parallel orientation of primary dendrites can also be seen in the ganglion cell layer of carp, probably reflecting several growth processes in the retina (Kock and Reuter, 1978).

The Polyaxons in TAC Networks

In an attempt to determine a plausible mechanism for our findings, we at first considered a passive mechanism, driven by varying primary dendrite diameters (Goldstein and Rall, 1974), as has been used to explain velocity differences. Such a relation has been observed in both intra- and extraretinal neurones (e.g., Pumphery and Young, 1938; Stone and Freeman, 1971) and is used as the basis for ganglion cell classification in goldfish (Northmore and Oh, 1998). However, a 4–5-fold, systematic and directional difference in dendrite diameters within receptive field areas is required to explain the average TAC velocity asymmetry, assuming a purely passive conduction through the network. Our examination of tracer-coupled networks does not conform to this hypothesis.

Even though the primary dendritic tree appears to be symmetric, the polyaxonal network (Cook and Werblin 1994; Taylor, 1996; Völgyi et al., 2001) does not (Teranishi et al., 1987; Djamgoz et al., 1990). In cyprinids, temporal properties of amacrine cell responses have previously been linked to the polyaxonal system (Djamgoz et al., 1990), however these systems per se appear to be oriented but not directed (Djamgoz et al., 1989, Fig. 12). Thus, these processes probably cannot, without further refinement, provide the platform needed for a direction-selective mechanism.

The polyaxons in carp frequently exhibit varicosities along their length. The complexity of these varicosity-laden processes as a candidate of local synaptic transmission has been demonstrated in retinal amacrine cells (e.g., Ellias and Stevens, 1980; Famiglietti, 1991; Freed et al., 1996) and in the direction-sensitive circuitry of rabbit retina (Famiglietti, 2002; Fried et al., 2002). Briefly, the varicosities in amacrine cells contain inputs and outputs to the bipolar cell layer (e.g., Ellias and Stevens 1980; Famiglietti, 1991) and/or ganglion cell layer (Famiglietti, 1992, 2002; Dacheux et al., 2003); in carp, the close spacing of the varicosities along a polyaxon makes them effectively cover the input from bipolar cells along their length. The large number of input/output sites implies that the process acts over a large number of synapses, distributed at near-equal intervals, which preserves the approximately linear distance-latency relationship observed. Most importantly, studies in hippocampal cortex (Raastad and Shepherd, 2003) and retinal ganglion cells (Fohlmeister and Miller, 1997) suggest that this type of thin varicosity-laden axon conducts signals with high reliability, making it especially suitable for long-range signal transmission over a large receptive field.

A Model for the Temporal Asymmetry and Displacement of Amplitude Center

The varicosity-laden processes (Fig. 1, C and D) showed a strong directionality, which coincided with the direction of the velocity asymmetry. Based on the appearance of the polyaxonal network, we propose a model for TACs to explain both the asymmetry in conduction velocity and the displacement of the location of the maximum amplitude (Fig. 8).

In the model we assume that a signal from the periphery of the receptive field of a TAC interacts with the soma region of the cell along two routes. (a) Dendrites and gap junctions between the TAC somata, which form a more or less symmetric syncytium. (b) A long thin polyaxonal process with distinct varicosities (compare also Fig. 1, C and D) in one direction from the soma, to the right in Fig. 8 A. In line with previous findings (e.g., Ellias and Stevens, 1980; Ishizuka et al., 1990), we suggest that the varicosities define locations of synaptic contacts of the long process with bipolar axon terminals, to act locally to decrease bipolar input to TACs and the conductance within the TAC dendritic network.

In this model, the axonal output is suggested to be represented by γ-aminobutyric acid (GABA), as goldfish TACs are mainly GABAergic (Watanabe et al., 2000) and signal propagation in separate amacrine cell network domains can be regulated by GABA (Yamada et al., 2002). Likewise, due to the known strong involvement in bipolar cells (Murakami et al., 1975; Kondo and Toyoda, 1980; Nawy and Copenhagen, 1990), glutamate is the most likely transmitter candidate to be regulated; however, other neurotransmitters could also

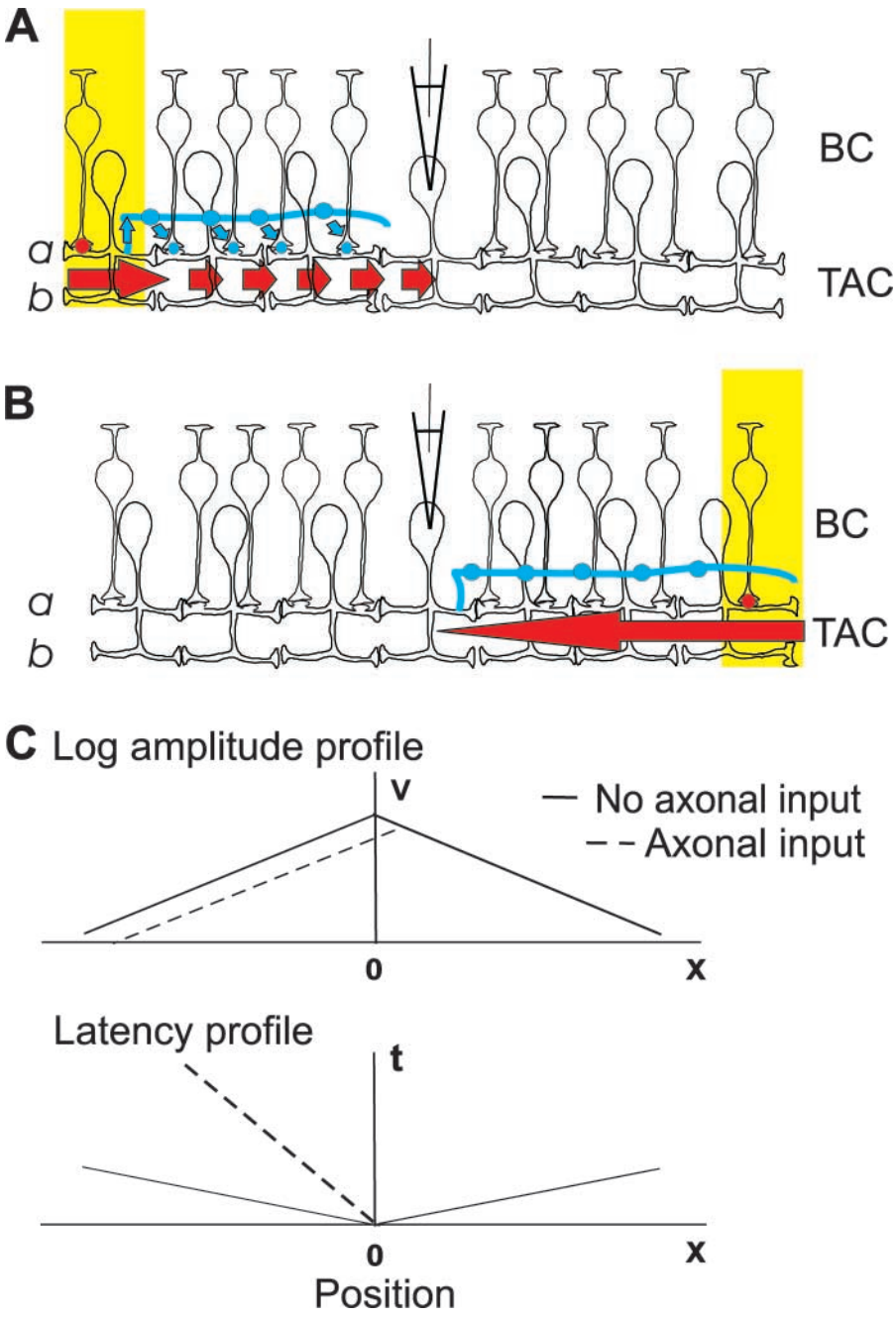

FIGURE 8. Schematic diagram of a polyaxonal inhibition model in TACs. The model assumes a negative input from polyaxons of TACs to the TAC network via bipolar cell axon terminals at the inner plexiform layer. In this figure, only inputs through sublamina *a* are depicted for clarity. (A) At a light-induced stimulus (yellow area to the left corresponding to a slit on the surface of the retina), a TAC (to the left) receives an excitatory signal (red dot) from the bipolar cell layer and sends it toward the electrode (red arrows). A directed axonal process (as shown by a blue line) sends an inhibitory input through bipolar cell axon terminals to other TACs (blue arrows). Due to the speed of the signal propagation in the axon, this inhibitory input decreases the conductance of the dendritic network before the arrival of the dendritic signal, thus resulting in a decrease of the conduction speed of the signal (shortening of red arrows). (B) The same situation as in A, but here the signal arrives from the right side toward the electrode only through the dendritic syncytium. In this case, any axonal signal elicited by the light stimulus will go in the opposite direction, from the electrode and not be able to affect measured latencies and amplitudes (unchanged red signal arrow). (C) Effects of the feedback on the amplitude and latency profile of the TAC. The situation with an axonal input is shown by a dotted line, compared with the situation without axon shown by a solid line. Both effects amplify the observed asymmetry. The decrease of the response amplitude shifts the amplitude peak toward it (to the right in this figure). The depression of transmitter release from bipolar cell axon terminals selectively decreases the plasma-membrane conductance of TACs (in the left side of this figure), resulting in the deceleration of the conduction velocity on this side of the receptive field.

be responsible for this interaction (Marshak, 1992). Thus, this straight and long process would provide a negative feedback or inhibiting channel, regulating local dendritic signal propagation from the soma of a cell toward the periphery of the dendritic field.

The effect of the polyaxonal inhibition depends strongly on the timing of the output (Fig. 8, A and B). If the light stimulus (slit) is on the ventral side (Fig. 8 A, left) of the recording electrode, then the cell(s) located at the stimulus send a signal through the fast-conducting polyaxon toward the electrode. Due to the speed of this signal, it will reach the bipolar terminals before the signal in the TAC dendrites along the axon, i.e., in the area containing both the axon and dendrite network. The axonal signal will act over the bipolar terminals and decrease the signal conduction in the TAC dendrite network. Thus, the signal from the dendritic network on the ventral side will arrive later at the electrode. On the other hand (Fig. 8 B), if the light stimulus is on the dorsal side (right-side in this figure), a transient dendritic signal propagating toward the electrode will be unaffected by axons, since any axonal effect on dendrites will occur after the signal has passed, due to the direction and starting point of the axons.

The effects of the inhibition on the receptive field properties are shown in Fig. 8 C. The decrease of the

response amplitude in a receptive field part would shift the amplitude peak away from this domain (here, to the right in Fig. 8); since the axonal input acts over a large number of synapses, distributed at approximately equal intervals over a large distance, the shift would tend to be a linear shift, as opposed to a one-point feedback. The suppression of glutamatergic transmitter release from bipolar cell axon terminals would selectively decrease the plasmamembrane conductance of TACs (in the left side of Fig. 8), resulting in a reduction of the conduction velocity on this side of the receptive field. Thus, this model could explain our observations about the response properties in the receptive field.

A Role for Direction Selectivity?

Directional selectivity and sensitivity has been observed throughout the retinal structures (DeVoe et al., 1989, Ammermüller et al., 1995). Recently, several papers (Taylor et al., 2000; Borg-Graham, 2001; Taylor and Vaney, 2002; Euler et al., 2002; Fried et al., 2002) have addressed the question of the location of the mechanism controlling ganglion cell directional sensitivity in mammals as based on the classical model of shunting inhibition by Torre and Poggio (1978). Here, the circuitry used a timing delay to combine input signals. The main mechanisms are believed to be either postsynaptical (Taylor et al., 2000) and/or presynaptical processing (Borg-Graham, 2001; Euler et al., 2002; Taylor and Vaney, 2002).

In carp, the observed conduction velocities in TACs are attributable to a presynaptic process with changing delay, which depends on the direction of the movement of the object. Currently, the precise synaptology between TACs and ganglion cells in carp is not known. Many findings strongly suggest that inputs from TACs onto ganglion cells are functionally inhibitory (Miller and Dacheux, 1976; Thibos and Werblin, 1978; Wunk and Werblin, 1979; Frumkes et al., 1981). Other findings, however, suggest that TACs send an excitatory input to On-Off ganglion cells in catfish (Sugawara, 1985; Sakai and Naka, 1987). Therefore, the question of whether TACs could provide a basis for an inhibitory or an excitatory presynaptic model, remains still open for debate. Pharmacologically, GABA is a common factor in this circuitry, as its antagonists abolish the direction selectivity of ganglion cells (in rabbit, Wyatt and Daw, 1976; Ariel and Daw, 1982; Kittila and Massey, 1997) and goldfish TACs are mainly GABAergic (Watanabe et al., 2000). Further studies are needed to elucidate the mechanisms responsible for the temporal delay circuitry.

Direction Selectivity Among Carp Ganglion Cells

As mentioned, in rabbit, there are a number of studies focusing on direction selectivity in the inner retina. Despite the evidence of orientation- and direction-tuned cells in higher visual centers, such as in the optic tectum (Cronly-Dillon, 1964; Jacobson and Gaze, 1964; Riemschlag and Schellart, 1978), the only detailed, published study about direction-selective ganglion cells in carp (or goldfish) appears to be a paper published by Bilotta and Abramov (1989). Here, half of the recorded cells (Y- and W-class ganglion cells) showed direction tuning. In the reported cases, the width of the peak in direction tuning was ~60 degrees and the tuning observed here was qualitatively different from the orientation tuning they could observe.

The Absent Bipolar-amacrine Feedback Response

A crucial factor for the range of any amacrine-bipolar cell feedback is the signal spread within the bipolar cell network, i.e., in this work the part affected by a varicosity-linked feedback. To date, we are not aware of any verified TAC input signals recorded in bipolar cells, despite the morphologically well-established existence of reciprocal synapses. This could be due to various factors, such as the narrowness of the soma-terminal connection, in combination with calcium buffers or calcium-dependent enzymes, e.g., PKC, in the terminal (Negishi et al., 1988; Suzuki and Kaneko, 1990), or control of terminal calcium currents (Freed et al., 2003; in cones, Hirasawa and Kaneko, 2003).

Other Cell Populations Coupled to TACs

The other populations in our stainings did not bear apparent resemblance to previously described amacrine cell groups in carp (Teranishi et al., 1987); however, in some cases the appearances matched those of sustained amacrine and interstitial cells found in goldfish (Djamgoz et al., 1990). The precise synaptic connectivity and distribution of these cells, other than their neurobiotin coupling to TACs, are unknown. With respect to the coupling to TACs, the presence of these populations varied considerably between specimens, without obvious patterns. Their gap junctional connections to TACs appear to be heterologous (Mills and Massey, 2000; for review, see e.g., Vaney and Weiler, 2000); thus, these connections should have a lower permeability (Massey and Mills, 1999; Mills and Massey, 2000) and lower connexon conductivity (Dermietzel et al., 2000) than the homologous coupling within the TAC network, decreasing the importance of heterologous connections to TACs as current conductors.

Capture of Object Movements

As the recorded conduction velocities constitute the speed for signals crossing the retinal plane, it is imperative that their range exceeds or at least matches the expected speeds of objects in natural surroundings. In our case, peak velocities of 100–120 mm/s on the reti-

nal surface of a 12-mm size eye ball corresponds approximately to a passage time of 100 ms for an object crossing over 60 degrees in the visual field. Also, the low-end average velocity of ~24 mm/s corresponds to 500 ms for the same object. This range would encapsulate a significant proportion of the movements occurring in nature.

The Orientation of the Fast-Slow Velocity Axis

The importance of the systematically oriented velocity profile may be found in its relation to the outer world. In carp TACs, the recorded velocity profiles contribute to an asymmetric signal along the vertical axis, whereas the left-right stimulation remains symmetric. A class of sustained amacrine cells in catfish respond much more intensely to bars moving vertically rather than horizontally (Naka, 1980), and both amplitude distribution and dendritic field of these cells exhibited asymmetric spatial properties. These types of vertical-horizontal asymmetries possibly reflect the up-down asymmetry of the ambient light level in the aquatic environment. Also, while mammalian starburst cells cover the retina several tenfold (Tauchi and Masland, 1984; Vaney, 1984), the strongly coupled TAC apparently has a low coverage factor, which may restrict its capabilities to deal with direction selectivity.

These findings link cellular functions to simple forms of direction and orientation detection. We suggest that they may form an evolutionary intermediate step toward the more refined forms of orientation and direction selectivity.

We are grateful to Dr. Soh Hidaka for advice with the neurobiotin staining; Dr. Richard Shiells and Professor Tom Reuter for correction of our manuscript; Professors Kristian Donner and David Marshak, Drs. Kaoru Katoh, Tomas van Groen, and Riitta Miettinen for valuable discussions and comments; to Mr. Kei Tomita and M.Sc. Hajime Hirasawa for technical assistance; and Dr. Ewen Macdonald for revising the language.

We would also like to thank the Science and Technology Agency of Japan (Project: Studies on the controlling factors for regeneration of the retinal circuitry and the optic nerve) and the Finska Läkaresällskapet for financial support.

Olaf S. Andersen served as editor.

Submitted: 14 March 2003
Accepted: 25 August 2003

REFERENCES

Ammermüller, J., J.F. Muller, and H. Kolb. 1995. The organization of the turtle inner retina. II. Analysis of color-coded and directionally selective cells. *J. Comp. Neurol.* 358:35–52.

Ariel, M., and N.W. Daw. 1982. Pharmacological analysis of directionally sensitive rabbit retinal ganglion cells. *J. Physiol.* 324:161–185.

Barlow, H.B., and W.R. Levick. 1965. The mechanism of directionally selective units in rabbit retina. *J. Physiol.* 178:477–504.

Bilotta, J., and I. Abramov. 1989. Orientation and direction tuning of goldfish ganglion cells. *Vis. Neurosci.* 2:3–13.

Bloomfield, S.A. 1992. Relationship between receptive and dendritic field size of amacrine cells in rabbit retina. *J. Neurophysiol.* 68:711–725.

Bloomfield, S.A. 1996. Effect of spike blockade on the receptive-field size of amacrine and ganglion cells in the rabbit retina. *J. Neurophysiol.* 75:1878–1893.

Borg-Graham, L. 2001. The computation of directional selectivity in the retina occurs presynaptic to the ganglion cells. *Nat. Neurosci.* 4:176–183.

Cook, P.B., and F.S. Werblin. 1994. Spike initiation and propagation in wide field transient amacrine cells of the salamander retina. *J. Neurosci.* 14:3852–3861.

Cronly-Dillon, J.R. 1964. Units sensitive to direction of movement in goldfish optic tectum. *Nature.* 203:214–215.

Dacheux, R.F., M.F. Chimento, and F.R. Amthor. 2003. Synaptic input to the on-off directionally selective ganglion cell in the rabbit retina. *J. Comp. Neurol.* 456:267–278.

Dermietzel, R., M. Kremer, G. Paputsoglu, A. Stang, I.M. Skerrett, D. Gomes, M. Srinivas, U. Janssen-Bienhold, R. Weiler, B.J. Nicholson, et al. 2000. Molecular and functional diversity of neural connexins in the retina. *J. Neurosci.* 20:8331–8343.

DeVoe, R.D., P.L. Carras, M.H. Criswell, and R.G. Guy. 1989. Not by ganglion cells alone: direction selectivity is widespread in identified cells of the turtle retina. *In* Neurobiology of the Inner Retina. R. Weiler and N.N. Osborne, editors. Springer, Berlin. 235–246.

Detwiler, P.B., A.L. Hodgkin, and P.A. McNaughton. 1978. A surprising property of electrical spread in the network of rods in the turtle's retina. *Nature.* 274:562–565.

Djamgoz, M.B.A., J.E.G. Downing, and H.-J. Wagner. 1989. Amacrine cells in the retina of a cyprinid fish: functional characterization and intracellular labelling with horseradish peroxidase. *Cell Tissue Res.* 256:607–622.

Djamgoz, M.B.A., L. Spadavecchia, C. Usai, and S. Vallerga. 1990. Variability of light-evoked response pattern and morphological characterization of amacrine cells in goldfish retina. *J. Comp. Neurol.* 301:171–190.

Djupsund, K., and M. Yamada. 1997. Asymmetric temporal properties within the receptive field of transient amacrine cells. *Neurosci. Res.* 21:1622.

Donner, K., K. Djupsund, T. Reuter, and I. Virtanen. 1991. Adaptation to light fluctuations in the frog retina. *Neurosci. Res.* 15: S175–S184.

Ellias, S.A., and J.K. Stevens. 1980. The dendritic varicosity: a mechanism for electrically isolating dendrites of cat retinal amacrine cells? *Brain Res.* 196:365–372.

Euler, T., P.B. Detwiler, and W. Denk. 2002. Directionally selective calcium signals in dendrites of starburst amacrine cells. *Nature.* 418:845–852.

Famiglietti, E.V., Jr. 1991. Synaptic organization of starburst amacrine cells in rabbit retina: analysis of serial thin sections by electron microscopy and graphic reconstruction. *J. Comp. Neurol.* 309: 40–70.

Famiglietti, E.V., Jr. 1992. Dendritic co-stratification of ON and ON-OFF directionally selective ganglion cells with starburst amacrine cells in rabbit retina. *J. Comp. Neurol.* 324:322–335.

Famiglietti, E.V., Jr. 2002. A structural basis for omnidirectional connections between starburst amacrine cells and directionally selective ganglion cells in rabbit retina, with associated bipolar cells. *Vis. Neurosci.* 19:145–162.

Fohlmeister, J.F., and R.F. Miller. 1997. Mechanisms by which cell geometry controls repetitive firing in retinal ganglion cells. *J. Neurophysiol.* 78:1948–1964.

Freed, M.A., R. Pflug, H. Kolb, and R. Nelson. 1996. ON-OFF amacrine cells in cat retina. *J. Comp. Neurol.* 364:556–566.

Freed, M.A., R.G. Smith, and P. Sterling. 2003. Timing of quantal

release from the retinal bipolar terminal is regulated by a feedback circuit. *Neuron*. 38:89–101.

Fried, S.I., T.A. Münch, and F.S. Werblin. 2002. Mechanisms and circuitry underlying directional selectivity in the retina. *Nature*. 420:411–414.

Frumkes, T.E., R.F. Miller, M. Slaughter, and R.F. Dacheux. 1981. Physiological and pharmacological basis of GABA and glycine action on neurones of mudpuppy retina. III. Amacrine-mediated inhibitory influences on ganglion cell receptive field organization: a model. *J. Neurophysiol.* 45:783–804.

Fukuda, Y., M. Watanabe, K. Wakakuwa, H. Sawai, and K. Morigiwa. 1988. Intraretinal axons of ganglion cells in the Japanese monkey (*Macaca fuscata*): conduction velocity and diameter distribution. *Neurosci. Res.* 6:53–71.

Goldstein, S.S., and W. Rall. 1974. Changes of potential shape and velocity for changing core conductor geometry. *Biophys. J.* 14: 731–757.

Hack, I., and L. Peichl. 1999. Horizontal cells of the rabbit retina are non-selectively connected to the cones. *Eur. J. Neurosci.* 11: 2261–2274.

Hidaka, S., M. Maehara, O. Umino, Y. Lu, and Y. Hashimoto. 1993. Lateral gap junction connections between retinal amacrine cells summating sustained responses. *Neuroreport.* 5:29–32.

Hirasawa, H., and A. Kaneko. 2003. External proton mediates the feedback from horizontal cells to cones in the newt retina. *In* The Neural Basis of Early Vision. A. Kaneko, editor. Springer, Tokyo, Berlin. 108–109.

Hsiao, C.-F., M. Watanabe, and Y. Fukuda. 1984. The relation between axon diameter and axonal conduction velocity of Y, X and W cells in the cat retina. *Brain Res.* 309:357–361.

Ishizuka, N., J. Weber, and D.G. Amaral. 1990. Organization of intrahippocampal projections originating from CA3 pyramidal cells in the rat. *J. Comp. Neurol.* 295:580–623.

Jacobson, M., and R.M. Gaze. 1964. Types of visual response from single units in the optic tectum and the optic nerve of the goldfish. *Q. J. Exp. Physiol.* 49:199–209.

Kaneko, A. 1973. Receptive field organization of bipolar and amacrine cells in the goldfish retina. *J. Physiol.* 235:133–153.

Kittila, C.A., and S.C. Massey. 1997. Pharmacology of directionally selective ganglion cells in the rabbit retina. *J. Neurophysiol.* 77: 675–689.

Kock, J.-H., and T. Reuter. 1978. Retinal Ganglion cells in the crucian carp (*Carassius carassius*). II. Overlap, shape and tangential orientation of dendritic trees. *J. Comp. Neurol.* 179:549–568.

Koizumi, A., S.-I. Watanabe, and A. Kaneko. 2001. Persistent Na^+ and Ca^{2+} current boost graded depolarization of rat retinal amacrine cells in culture. *J. Neurophysiol.* 86:1006–1016.

Kondo, H., and J.-I. Toyoda. 1980. Dual effect of glutamate and aspartate on the on-center bipolar cell in the carp retina. *Brain Res.* 199:240–243.

Kujiraoka, T., T. Saito, and J.-I. Toyoda. 1988. Analysis of synaptic inputs to ON-OFF amacrine cells in the carp retina. *J. Gen. Physiol.* 92:475–487.

Lamb, T.D., and S.J. Simon. 1976. The relation between intercellular coupling and electrical noise in turtle photoreceptors. *J. Physiol.* 263:257–286.

Marc, R.E., W.L.S. Liu, and J.F. Muller. 1988. Gap junctions in the inner plexiform layer of the goldfish retina. *Vision Res.* 28:9–24.

Marshak, D.W. 1992. Peptidergic neurons of teleost retinas. *Vis. Neurosci.* 8:137–144.

Masland, R.H., and A. Ames, III. 1976. Responses to acetylcholine of ganglion cells in an isolated mammalian retina. *J. Neurophysiol.* 39:1220–1235.

Massey, S.C., and S.L. Mills. 1999. Gap junctions between AII amacrine cells and calbindin-positive bipolar cells in the rabbit retina. *Vis. Neurosci.* 16:1181–1189.

Miller, R.F., and R.F. Dacheux. 1976. Synaptic organization and ionic basis of on and off channels in mudpuppy retina. III. A model of ganglion cell receptive field organization based on chloride-free experiments. *J. Gen. Physiol.* 67:679–690.

Miller, R.F., and S.A. Bloomfield. 1983. Electroanatomy of a unique amacrine cell in the rabbit retina. *Proc. Natl. Acad. Sci. USA*. 80: 3069–3073.

Mills, S.L., and S.C. Massey. 2000. A series of biotinylated tracers distinguishes three types of gap junction in retina. *J. Neurosci.* 20: 8629–8636.

Murakami, M., T. Otsuka, and H. Shimazaki. 1975. Effects of aspartate and glutamate on the bipolar cells in the carp retina. *Vision Res.* 15:456–458.

Naka, K.-I. 1980. A class of catfish amacrine cells responds preferentially to objects which move vertically. *Vision Res.* 20:961–965.

Naka, K.-I., and B.N. Christensen. 1981. Direct electrical connections between transient amacrien cells in the catfish retina. *Science.* 214:462–464.

Nawy, S., and D.R. Copenhagen. 1990. Intracellular cesium separates two glutamate conductances in retinal bipolar cells of goldfish. *Vision Res.* 30:967–972.

Negishi, K., S. Kato, and T. Teranishi. 1988. Dopamine cells and rod bipolar cells contain protein kinase C-like immunoreactivity in some vertebrate retinas. *Neurosci Lett.* 94:247–252.

Negishi, K., T. Teranishi, H. Sugawara, and H.-J. Wagner. 1991. Dendritic contacts between neighboring homologous amacrine cells in carp retina. *Neurosci. Res. Supp.* 15:S145–S155.

Northmore, D.P.M., and D.-J. Oh. 1998. Axonal conduction velocities of functionally characterized retinal ganglion cells in goldfish. *J. Physiol.* 506:207–217.

Pumphery, R.J., and J.Z. Young. 1938. Rates of conduction of nerve fibers of various diameters in cephalopods. *J. Exp. Biol.* 15:453–458.

Raastad, M., and G.M.G. Shepherd. 2003. Single-axon action potentials in the rat hippocampal cortex. *J. Physiol.* 548:745–752.

Riemschlag, F.C.C., and N.A.M. Schellart. 1978. Evoked potentials and spike responses to moving stimuli in the optic tectum of goldfish. *J. Comp. Physiol.* 128:13–20.

Sakai, H., and K.-I. Naka. 1987. Signal transmission in the catfish retina. IV. Transmission to ganglion cells. *J. Neurophysiol.* 58: 1307–1328.

Sakai, H.M., H.M. Machuca, and K.-I. Naka. 1997. Processing of color and noncolor-coded signals in the gourami retina II. Amacrine cells. *J. Neurophysiol.* 78:2018–2033.

Shiells, R.A., and G. Falk. 2000. Activation of Ca^{2+}-calmodulin kinase II induces desensitization by background light in dogfish retinal 'on' bipolar cells. *J. Physiol.* 528: 327–338.

Smirnakis, S.M., M.J. Berry, D.K. Warland, W. Bialek, and M. Meister. 1997. Adaptation of retinal processing to image contrast and spatial scale. *Nature.* 386:69–73.

Stell, W.K., and F.I. Harosi. 1976. Cone structure and visual pigment content in the retina of the goldfish. *Vision Res.* 16:647–657.

Stone, J., and R.B. Freeman, Jr. 1971. Conduction velocity grouping in the cat optic nerve classified according to their retinal origin. *Exp. Brain Res.* 13:489–497.

Sugawara, K. 1985. Lateral actions at the inner plexiform layer of the carp retina: effects of turning windmill pattern stimulus. *Vision Res.* 25:1179–1186.

Suzuki, S., and A. Kaneko. 1990. Identification of bipolar cell subtypes by protein kinase C-like immunoreactivity in the goldfish retina. *Vis. Neurosci.* 5:223–230.

Tauchi, M., and R.H. Masland. 1984. The shape and arrangement of the cholinergic neurons in the rabbit retina. *Proc. R. Soc. Lond.*

B. Biol. Sci. 223:101–119.
Taylor, W.R. 1996. Response properties of long-range axon-bearing amacrine cells in the dark-adapted rabbit retina. *Vis. Neurosci.* 13: 599–604.
Taylor, W.R., S. He, W.R. Levick, and D.I. Vaney. 2000. Dendritic computation of direction selectivity by retinal ganglion cells. *Science.* 289:2347–2350.
Taylor, W.R., and D.I. Vaney. 2002. Diverse synaptic mechanisms generate direction selectivity in the rabbit retina. *J. Neurosci.* 22: 7712–7720.
Teranishi, T., K. Negishi, and S. Kato. 1987. Functional and morphological correlates of amacrine cells in carp retina. *Neuroscience.* 20:935–950.
Thibos, L.N., and F.S. Werblin. 1978. The response properties of the steady antagonistic surround in the mudpuppy retina. *J. Physiol.* 278:79–99.
Torre, V., and T. Poggio. 1978. A synaptic mechanism possibly underlying directional selectivity to motion. *Proc. R. Soc. Lond. B. Biol. Sci.* 202:409–416.
Vaney, D.I. 1984. 'Coronate' amacrine cells in the rabbit retina have the 'starburst' dendritic morphology. *Proc. R. Soc. Lond. B. Biol. Sci.* 220:501–508.
Vaney, D.I., and R. Weiler. 2000. Gap junctions in the eye: evidence for heteromeric, heterotypic and mixed-homotypic interactions. *Brain Res. Brain Res. Rev.* 32:115–120.
Völgyi, B., D. Xin, Y. Amarillo, and S.A. Bloomfield. 2001. Morphology and physiology of the polyaxonal amacrine cells in the rabbit retina. *J. Comp. Neurol.* 440:109–125.
Watanabe, S.-I., A. Koizumi, S. Matsunaga, J.W. Stocker, and A. Kaneko. 2000. GABA-mediated inhibition between amacrine cells in the goldfish retina. *J. Neurophysiol.* 84:1826–1834.
Watanabe, S.-I., and M. Murakami. 1985. Electrical properties of ON-OFF transient amacrine cells in the carp retina. *Neurosci. Res. Suppl.* 2:S201–S210.
Wunk, U.F., and F.S. Werblin. 1979. Synaptic inputs to the ganglion cells in the tiger salamander retina. *J. Gen. Physiol.* 73:265–286.
Wyatt, H.J., and N.D. Daw. 1976. Specific effect of neurotransmitter antagonists on ganglion cells in rabbit retina. *Science.* 191:204–205.
Yagi, T. 1986. Interaction between the soma and axon terminal of retinal horizontal cells in Cyprinus carpio. *J. Physiol.* 375:121–135.
Yamada, M., Y. Shigematsu, Y. Umetani, and T. Saito. 1992. Dopamine decreases receptive field size of rod-driven horizontal cells in carp retina. *Vision Res.* 32:1801–1807.
Yamada, M., and T. Saito. 1997. Dual component in receptive field centre of bipolar cells in carp retina. *Vision Res.* 37:2331–2338.
Yamada, Y., A. Koizumi, E. Iwasaki, S.-I. Watanabe, and A. Kaneko. 2002. Propagation of action potentials from the soma to individual dendrite of cultured rat amacrine cells is regulated by local GABA input. *J. Neurophysiol.* 87:2858–2866.
Yang, G., and R. Masland. 1994. Receptive fields and dendritic structure of directionally selective retinal ganglion cells. *J. Neurosci.* 14:5267–5280.